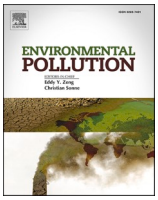
Environmental Pollution 348 (2024) 123803



Contents lists available at ScienceDirect

Environmental Pollution

journal homepage: www.elsevier.com/locate/envpol





Assessing the role of cold front passage and synoptic patterns on air pollution in the Korean Peninsula☆

Jung-Woo Yoo [a], Soon-Young Park [b], Hyun-Young Jo [a], Yeomin Jeong [a], Hyo-Jung Lee [a,c], Cheol-Hee Kim [a,c], Soon-Hwan Lee [a,d,*]

[a] Institute of Environmental Studies, Pusan National University, Busan, 46241, Republic of Korea
[b] Department of Science Education, Daegu National University of Education, Daegu, 42411, Republic of Korea
[c] Department of Atmospheric Sciences, Pusan National University, Busan, 46241, Republic of Korea
[d] Department of Earth Science Education, Pusan National University, Busan, 46241, Republic of Korea

ARTICLE INFO

Keywords:
Cold front
Low-pressure
Subsidence
Non-stationary
$PM_{2.5}$

ABSTRACT

Various numerical experiments using WRF (Weather Research & Forecasting Model) and CMAQ (Community Multiscale Air Quality Modeling System) were performed to analyze the phenomenon of rapidly high concentration $PM_{2.5}$ after the passage of a cold front in an area with limited local emissions. The episode period was from January 14 to 23, 2018, and analysis was conducted by dividing it into two stages according to the characteristics of changes in $PM_{2.5}$ concentrations during the period. Through the analysis of observational data during the episode period, we confirmed meteorological impacts (decrease in temperature, increase in wind speed and relative humidity) and an increase in air pollution (PM_{10} and $PM_{2.5}$) attributed to the passage of a cold front. Using CMAQ's IPR (Integrated Process Rate) analysis, the contribution of the horizontal advection process was observed in transporting $PM_{2.5}$ to Gangneung at higher altitudes, and the $PM_{2.5}$ concentrations at the surface increased because the vertical advection process was influenced by the terrain. Notably, in Stage 2 (64 $\mu g \cdot m^{-3}$), a higher contribution of the vertical advection process compared to Stage 1 (35 $\mu g \cdot m^{-3}$) was observed, which is attributed to the differences in synoptic patterns following the passage of the cold front. During Stage 2, following the cold front, atmospheric stability (dominance of high-pressure system) led to air subsidence and the presence of a temperature inversion layer, creating favorable meteorological conditions for the accumulation of air pollutants. This study offers the mechanisms of air pollution over the Korean Peninsula under non-stationary meteorological conditions, particularly in relation to the passage of the cold front (low-pressure system). Notably, the influence of a cold front can vary according to the synoptic patterns that develop following its passage.

1. Introduction

Air pollution is a significant public health issue, negatively impacting human health and ecosystems (Cohen et al., 2017; Apte et al., 2018; Agathokleous et al., 2020). The primary causes of air pollution are known to be emissions of pollutants primarily originating from human activities and are influenced by meteorological conditions and topographical factors. In particular, meteorological conditions have been shown to contribute more than 30–50% to the occurrence of severe air pollution events (Zhang et al., 2018; Ma et al., 2020). Meteorological conditions, such as wind, planetary boundary layer (PBL) heights, relative humidity, temperature, and air stagnation, affect the transport, accumulation, dispersion, and chemical reactions of pollutants (Tai et al., 2010; Pateraki et al., 2012; Chen et al., 2018).

Air pollution frequently occurs under meteorological conditions dominated by high-pressure systems. The dominance of high-pressure systems leads to meteorological stagnation characterized by low wind speeds and absence of precipitation. These meteorological conditions create a favorable environment for the surface accumulation of pollutants, contributing to the occurrence of air pollution (Liu et al., 2013; Li et al., 2015; Liu et al., 2019; Bei et al., 2020; Jun and Gu, 2023).

Air pollution can occur under strong winds or non-stagnant

☆ This paper has been recommended for acceptance by Prof. Pavlos Kassomenos.

* Corresponding author. Institute of Environmental Studies, Pusan National University, Busan, 46241, Republic of Korea.
E-mail address: withshlee@pusan.ac.kr (S.-H. Lee).

https://doi.org/10.1016/j.envpol.2024.123803
Received 13 January 2024; Received in revised form 26 February 2024; Accepted 14 March 2024
Available online 21 March 2024
0269-7491/© 2024 Elsevier Ltd. All rights reserved.

meteorological conditions (Yu et al., 2020). In East Asia, where prevailing westerly winds dominate, strong winds in the lower atmosphere can cause the long-range transport of pollutants from upwind areas, leading to air pollution in downwind areas (Itahashi et al., 2017; Lu et al., 2019; Yu et al., 2020; Hu et al., 2021; Mo et al., 2021). The development of lee trough-induced low-pressure systems at high altitudes enhances pollutant transport through strong winds (Yoo et al., 2022).

Additionally, low-pressure systems with cold fronts during the winter can influence air pollution. Cold fronts are formed when cold air moves in and pushes under warmer air, resulting in rapid changes in meteorological conditions, including temperature, wind, and air pressure. The increased wind speeds accompanying the passage of cold fronts can promote the dispersion of pollutants into adjacent areas, potentially resulting in improved air quality (Hu et al., 2018).

However, the passage of a cold front can induce air pollution in the downwind areas as pollutants are transported through advection processes (Zhang et al., 2022). Zeng et al. (2010) reported that dust events occur at high altitudes in northern China due to the strong winds associated with cold fronts. Furthermore, Hu et al. (2019) found that the air quality in downwind areas deteriorates due to the accumulation of pollutants along the edges of the cold front. Additionally, more than 60% of haze occurrences in some regions of China are attributed to long-range transport induced by cold fronts (Liu et al., 2021). Jin et al. (2021) proposed that the passage of a cold front or a low-pressure system can induce a strong upward flux through surface convergence, leading to the dispersion of surface pollutants into the upper-layer. Air pollutants in the upper-layer are then transported over long distances, leading to high concentrations in downwind areas (Kang et al., 2021). In addition, the atmosphere can be stabilized by a high-pressure system developing behind the cold front. Zhang et al. (2018) reported an increase in $PM_{2.5}$ concentrations when a low-pressure system transitioned to a high-pressure system.

Despite their potential to induce air pollution, low-pressure systems accompanying the cold front have not received significant attention in air pollution issues because of their association with precipitation and strong winds.

The Korean Peninsula is surrounded by seas on three sides and features complex mountainous terrain. This complexity in mountainous and coastline distributions leads to intricate processes related to precipitation development and front formations. In particular, when low-pressure systems encounter such complex terrain during their movement, they can become a key factor in determining the transport characteristics of air pollutants. Therefore, this study aimed to analyze the impact and characteristics of the occurrence of high concentration $PM_{2.5}$ and changes in concentrations due to the passage of the cold front in the complex mountainous and coastal terrain of the Korean Peninsula.

2. Methods

2.1. Air quality and meteorological data

Deterioration in air quality in regions with low local emissions may be influenced by long-range transport from upwind areas. We conducted an analysis of the Gangneung area, which has low local emissions and is located in the downwind area with mountainous terrain to the west, where changes in $PM_{2.5}$ concentrations may occur due to the passage of cold fronts (Fig. S1).

To investigate the air quality in Gangneung, we collected measured data on $PM_{2.5}$ hourly concentrations from the Air Quality Monitoring Station (AQMS) network managed by the National Institute of Environmental Research (http://www.airkorea.or.kr).

Meteorological observation data were obtained from the Automated Synoptic Observing System (ASOS) provided by the Korea Meteorological Administration (KMA). In this study, we investigated the passage of cold fronts and air quality using hourly 2-m temperature and relative humidity, and 10-m wind speed during winter (January, February, and December) from 2016 to 2022.

Observation data were collected to evaluate the performance of the meteorological and air quality numerical models. The results of the WRF (Weather Research & Forecasting Model) and CMAQ (Community Multiscale Air Quality Modeling System) models were statistically validated using ASOS meteorological observation data from 89 stations and AQMS air quality measurement data from 290 stations.

2.2. Reanalysis data

To analyze large-scale synoptic patterns during periods of high concentration in Gangneung, mean sea-level pressure (SLP) data from the winter of 2016–2022 were utilized. SLP data were obtained from the Final Operational Global Analysis (FNL) reanalysis dataset with a horizontal resolution of $0.25^\circ \times 0.25^\circ$ and temporal resolution of 6-hour (00, 06, 12, and 18 UTC) provided by the National Centers for Environmental Prediction (NCEP). The reanalysis data was utilized as both the initial and boundary data for the WRF model.

2.3. Model description

In this study, numerical simulations of meteorology and air quality were conducted using the WRF (version 3.9.1.1) model (Skamarock et al., 2008) and the CMAQ (version 5.2) model (Byun and Schere, 2006) to examine the impact of cold fronts on air quality. The simulation consisted of two domains: Domain 1 covered the East Asia region with a horizontal resolution of 27 km on a grid of 170×110 cells, and Domain 2 centered on the Korean Peninsula with 9 km resolution on a grid of 145×139 cells. In the vertical, the model was divided into a total of 40 layers. The WRF model's initial and boundary conditions are derived from the FNL reanalysis data. The simulation period covers from 10–24 January, with the initial 72-hour as spin-up time to mitigate the impact of uncertainties in the initial conditions.

Detailed physics options include the Morrison double-moment scheme (Morrison et al., 2009), the Noah Land Surface Model (Ek et al., 2003), the RRTMG shortwave and longwave schemes (Iacono et al., 2008), the Yonsei (YSU) University scheme (Hong et al., 2006), and Kain-Fritsch cumulus cloud parameterization (Kain, 2004). In this study, grid nudging was applied to obtain more accurate meteorological simulation results, particularly for synoptic patterns such as high- and low-pressure systems and fronts. Grid nudging was applied to both Domains 1 and 2 for the U and V wind components, potential temperature, and water-vapor mixing ratio above the PBL.

The anthropogenic emission data used in the CMAQ model were retrived from The Emissions Database for Global Atmospheric Research (EDGARv6.1), with a horizontal resolution of $0.1^\circ \times 0.1^\circ$. Additionally, biogenic emission data were sourced from the Model of Emissions of Gases and Aerosols from Nature (MEGAN version 2.1).

To quantitatively investigate the relationship between cold fronts and air quality, we utilized the Integrated Process Rate (IPR) derived from the Process Analysis (PA) module within the CMAQ model (Gipson and Young, 1999). IPR is utilized for identifying and quantifying the contributions of physical and chemical processes on air pollutants, including $PM_{2.5}$. These processes include (horizontal and vertical) advection and dispersion, emissions, chemical, aerosol, deposition, and cloud processes. The hourly contribution of each process was computed quantitatively. In this study, we analyzed the horizontal and vertical advection by considering the inflow and outflow of $PM_{2.5}$.

3. Results

3.1. $PM_{2.5}$ concentrations during the 2016–2022 winter

We investigated the temporal variations of $PM_{2.5}$ concentrations during winter from 2016 to 2022 in Gangneung, characterized by low

local emissions (Fig. S2). Consequently, we observed a decreasing trend in $PM_{2.5}$ concentrations, with a total of 16 days of severe air pollution cases (daily average $PM_{2.5} > 51$ μg·m^{-3}) recorded (Table S1). Severe air pollution occurred for 3 days in 2016 and peaked at 7 days in 2017. The number of occurrence days decreased after 2017, with no severe air pollution recorded from 2020 to 2022. The decreasing trend in severe air pollution occurrences is attributed to efforts to reduce anthropogenic emissions, both in South Korea and foreign countries (Zheng et al., 2018; Zhang et al., 2019; Bae et al., 2021).

To analyze the link between high $PM_{2.5}$ concentrations events in winter and large-scale synoptic patterns in Gangneung, we presented the mean sea-level pressure (SLP) distribution for the 8 days of severe air pollution occurrences (Fig. 2). Under the influence of high-pressure systems, air pollution tends to occur more frequently during elevated temperatures and stable atmospheric conditions. However, contrary to the expectation of wider isobar spacing due to the influence of high-pressure systems, the mean SLP distribution on days of high $PM_{2.5}$ concentrations events revealed densely spaced isobars. This result shows that the presence of a high-pressure system in the west and a low-pressure system in the east. A similar pressure pattern, with a low-pressure system present east of the Korean Peninsula, was also observed in the surface weather maps for high-concentration days (2016.01.04, 2016.12.05, 2017.01.18, 2017.01.19, 2018.01.16, 2018.01.17, 2018.01.20, 2019.01.15). This suggests that high-concentration $PM_{2.5}$ events can occur not only under well-known stable atmospheric conditions associated with high-pressure systems but also under dominant meteorological conditions influenced by low-pressure systems. Moreover, on all 8 days when low-pressure systems predominated over the Korean Peninsula, a decrease in temperature compared to the previous day was observed (Table S1). This suggests that severe air pollution may occur in Gangneung due to the influence of low-pressure systems accompanied by cold fronts. When considering Gangneung's geographical location in the downwind areas, pollutants may be transported from surrounding areas rather than originating from local emissions.

To examine the source of severe air pollution in Gangneung, we calculated 24-hour backward trajectories for 8 days using the Hybrid Single-particle Lagrangian Integrated Trajectory (HYSPLIT) model developed by the National Oceanic and Atmospheric Administration (NOAA). The analysis of backward trajectories revealed a predominant westerly trajectory (Fig. S3). As a result, pollutants from upwind areas (South Korea or foreign countries) are anticipated to be transported to Gangneung by westerly winds, potentially resulting in severe air pollution. Therefore, this study aims to investigate the relationship between meteorological changes due to the passage of cold fronts and the occurrence of severe air pollution in Gangneung.

3.2. Episode description

To investigate the influence of the cold front (low-pressure system) on high-concentration $PM_{2.5}$ during the winter season in Gangneung, we selected the period from January 14–23, 2018, as the study episode. During the episode, the daily average $PM_{2.5}$ concentrations reached a maximum of 64 μg·m^{-3} on the 20th, with an hourly average peaking at 97 μg·m^{-3} on the same day. On the 16th, 18th, and 20th, low-pressure systems appeared east of the Korean Peninsula (Fig. S4). In this study, we excluded the 18th day of precipitation from the analysis to eliminate the impact of precipitation on air quality. Therefore, focusing on the periods when low-pressure systems were present, we divided the analysis into two stages: (1) Stage 1: January 16, 00:00–1200 LST, and (2) Stage 2: January 19, 18:00–06:00 LST (January 20).

In Fig. 3, we present the observed data for Gangneung during the episode period, including PM_{10} and $PM_{2.5}$ concentrations as well as the meteorological data (2-m temperature and relative humidity, 10-m wind speed and direction). The shaded yellow area represents the periods of Stages 1 and 2. Fig. 3 reveals that during Stages 1 and 2, the 2-m temperature decreased while the 2-m relative humidity and 10-m wind speed increased. On January 15, the maximum 2-m temperature was recorded at 12.2 °C; however, it decreased to 7.0 °C on the 20th due to the influx of cold air. Additionally, the maximum temperature dropped by 0.9 °C on the 16th and 2.2 °C on the 20th compared to the previous day. The overall low relative humidity in Gangneung is attributed to the influence of the Siberian high-pressure system during winter on the Korean Peninsula. However, on the 17th, the relative humidity was higher owing to precipitation. During the passage of the cold front, the relative humidity increased from 25% to 41% on the 16th and from 20% to 47% on the 20th. Throughout the episode period (January 16–20), the daily average wind speed ranged from 1.9 to 3.1 m·s^{-1}. However, during the cold-front passage, the wind speed increased to 2–3 m·s^{-1}. For example, on the 16th, the wind speed increased from 1.5 m·s^{-1} (03:00 LST) to 5.1 m·s^{-1} (07:00 LST), resulting in a wind speed increase of 3.6 m·s^{-1}. Similarly, on the 20th, the wind speed increased from 0.7 m·s^{-1} (17:00 LST) to 4.7 m·s^{-1} (06:00 LST), resulting in a wind speed increase of 4.0 m·s^{-1}. Nevertheless, owing to the prevailing westerly winds typical of the Korean Peninsula during winter, changes in wind direction during the approach of the cold front were not pronounced. Additionally, the low-pressure system caused a decrease in the SLP of 3–7 hPa before and after the passage of the cold front (not shown).

During the episode period, three peaks in PM_{10} and $PM_{2.5}$ concentrations were observed in Gangneung, and an increase in concentrations occurred during the passage of the cold front. This suggests that the passage of the cold front may have affected the transport of pollutants and consequently caused the high concentrations in Gangneung. In Stage 1 (16th), the PM_{10} and $PM_{2.5}$ concentrations increased significantly from 40 μg·m^{-3} and 35 μg·m^{-3} at 22:00 LST on the 15th to 93 μg·m^{-3} and 64 μg·m^{-3} at 11:00 LST on the day of the cold front passage. In Stage 2 (20th), the $PM_{2.5}$ concentration started at 20 μg·m^{-3} at 00:00 LST and continued to rise, reaching 97 μg·m^{-3} at 13:00 LST, indicating an increase of 77 μg·m^{-3}. The concentration increase during Stage 2 was greater than that during Stage 1 and varied depending on the meteorological conditions.

3.3. Model performance evaluation

Successful WRF simulation results influence the production, advection, dispersion, and other aspects of air pollutants, thereby affecting the accuracy of CMAQ simulation results. Therefore, in this study, we compared the 2-m temperature and 10-m wind speed observed at ASOS meteorological observation stations in South Korea (red squares in Fig. 1) with the simulation results from the WRF to evaluate its performance (Fig. S5).

To evaluate the performance of the WRF simulation results compared to ASOS observation data, we employed statistical parameters, including mean bias (MB), Index of Agreement (IOA), and correlation coefficient (R). The 2-m temperature displayed a MB of −0.42 °C, indicating a slight underestimation compared to the observations. However, with an IOA of 0.95 and a R of 0.90, the results satisfied the criteria proposed by Emery et al. (2001) (Bias $\leq \pm 0.5$ °C; IOA ≥ 0.7). The simulation results for the 10-m wind speed slightly overestimated the observations with an MB of 1.50 m·s^{-1}. However, the IOA, at 0.68, well captured the trends and satisfied the baseline criteria suggested by Emery et al. (2001) (Bias ≤ 2.0 m·s^{-1}; IOA ≥ 0.6). Referring to a previous study (Emery et al., 2001), the meteorological predictions in this study demonstrated an overall reasonable model performance by accurately capturing the variability in the observed values. However, in this study, the WRF simulation results tended to slightly underestimate the 2-m temperature and overestimate the 10-m wind speed compared with the observations. Notably, the criteria proposed in a previous study (Emery et al., 2001) were based on predictions for flat regions. Therefore, they may allow for somewhat relaxed standards when applied to the complex terrain of the Korean Peninsula.

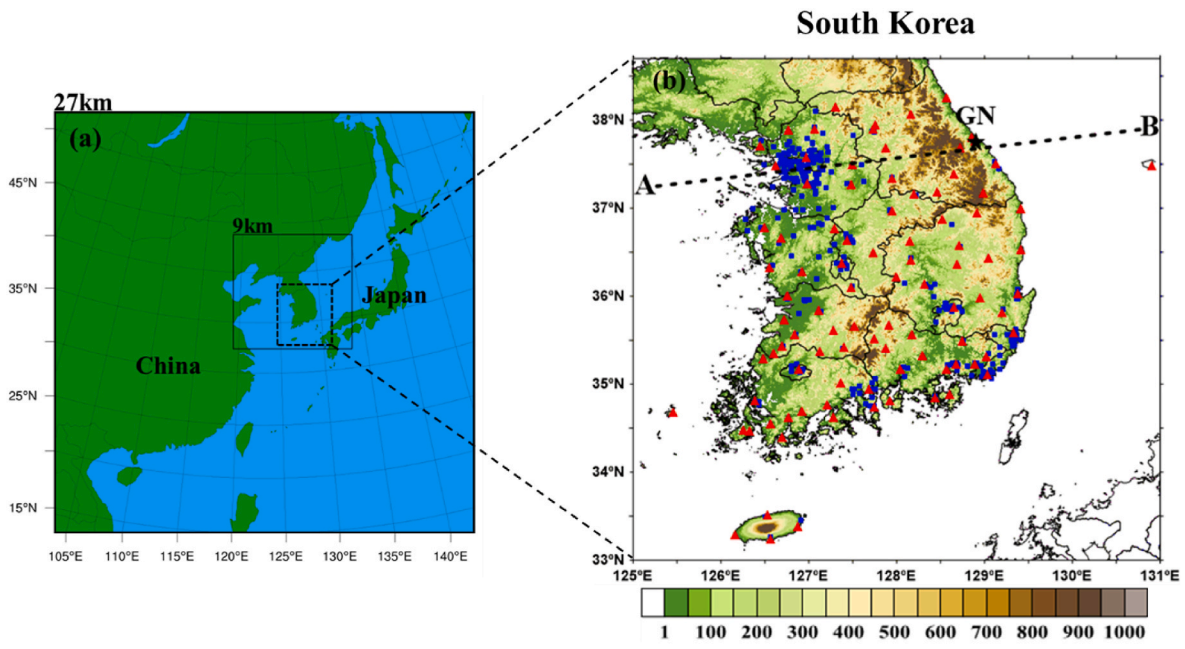


Fig. 1. (a) Study modeling domain for simulations and (b) terrain height (unit: m). Red triangles are the meteorological observation sites and blue circles are air quality measurement sites.

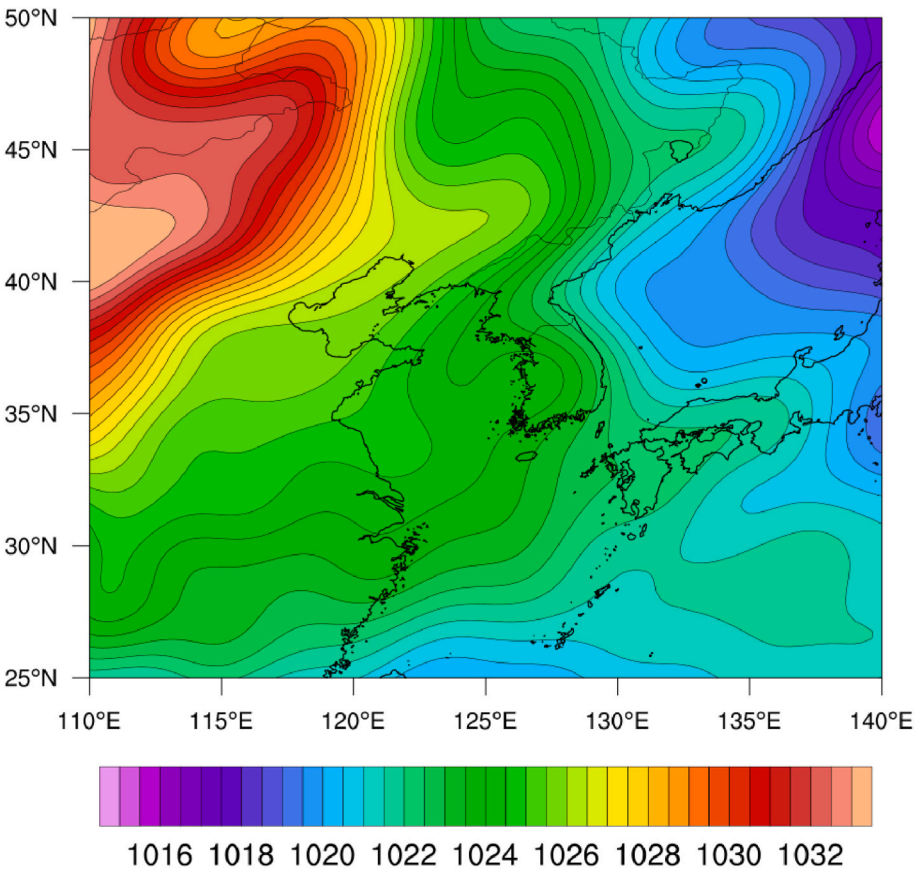


Fig. 2. Spatial distribution of mean sea-level pressure (units: hPa) during the period of exceeding of daily average $PM_{2.5}$ concentrations over 51 $\mu g \cdot m^{-3}$ in Gangneung from 2016 to 2020 winter.

Furthermore, the horizontal distribution of 2-m temperature changes over 24-hour showed a decrease of 2–4 °C in the central part of the Korean Peninsula, indicating that the temperature variations due to the passage of the cold front were well simulated (Fig. S6).

To evaluate the performance of the CMAQ simulation results, a statistical analysis was conducted by comparing the measured $PM_{2.5}$

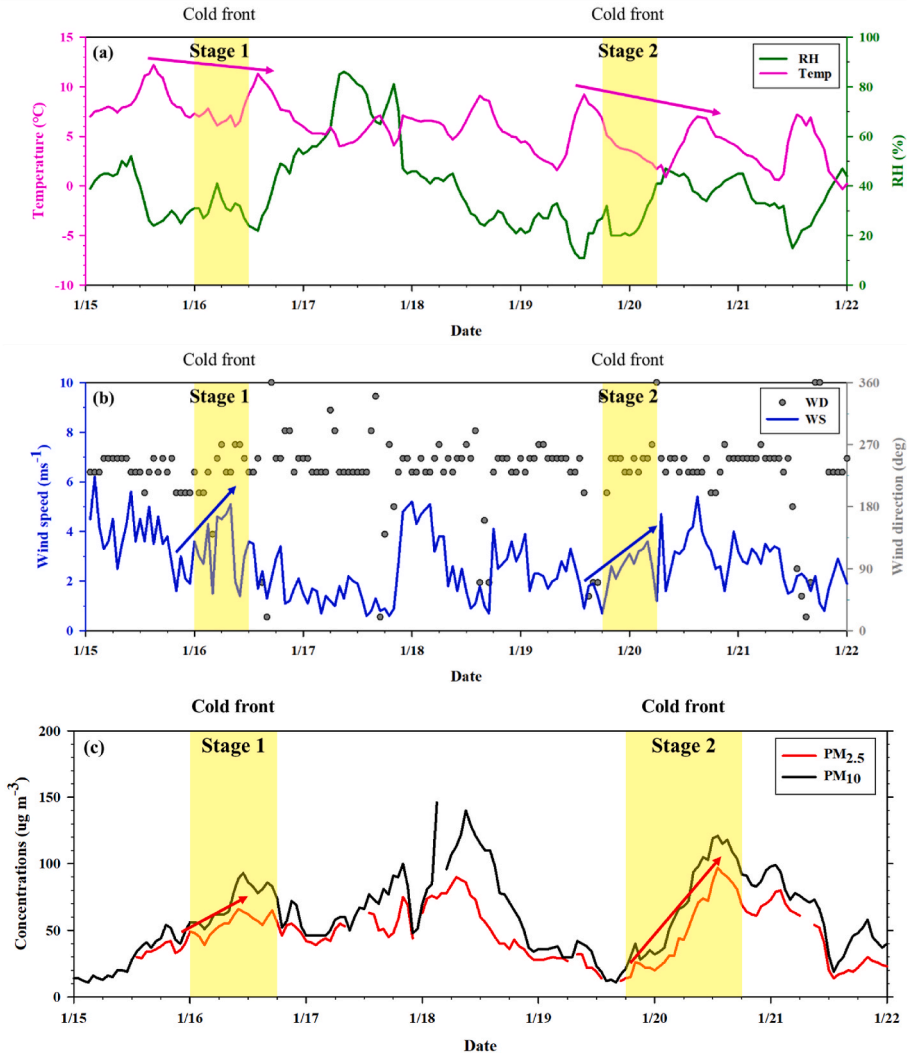


Fig. 3. Temporal variations of (a) temperature and Relative humidity at 2-m, (b) wind speed and direction at 10-m, and (c) PM_{10} and $PM_{2.5}$ concentrations at Gangneung.

concentrations from the AQMS in South Korea (blue circles in Fig. 1) with the CMAQ simulation results. The comparison of the temporal variations of the measured and CMAQ-simulated $PM_{2.5}$ concentrations during the episode period indicated that, in general, the model replicates the variability of the measured values well (Fig. S7). The performance of the simulated $PM_{2.5}$ displayed a tendency to underestimate with an MB of -12.79 μg·m^{-3}, but it effectively captured the variability with an IOA of 0.70. In the Gangneung area, the CMAQ simulation results effectively reproduced the $PM_{2.5}$ concentrations peak on the 16th; however, on the 20th, it appeared somewhat earlier (Fig. 4). This is believed to be due to the WRF simulation results overestimating the wind speed compared to the observations, causing $PM_{2.5}$ to be transported from abroad to South Korea more rapidly. The uncertainties in the CMAQ simulation results are attributed to uncertainties in the emission data, initial and boundary conditions, and meteorological simulation results (Miao et al., 2017). Overall, it appears that both the WRF and CMAQ results reasonably reproduced the variations in meteorology and $PM_{2.5}$. In addition, considering the similarity in timing between the approach of the cold front (low-pressure system) and the peak in $PM_{2.5}$ concentrations, we can infer that $PM_{2.5}$ was transported to South Korea and triggered high

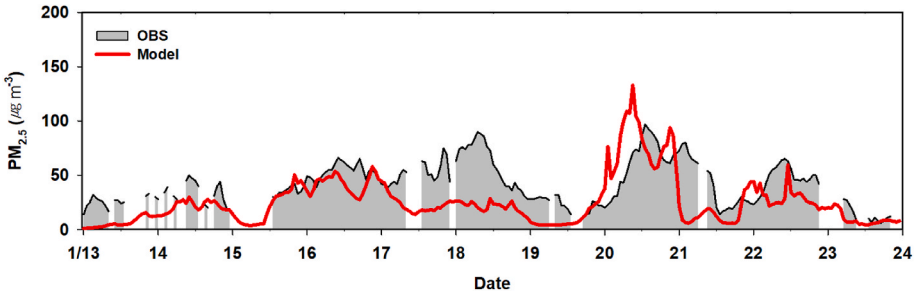


Fig. 4. Time series of measured (OBS) and simulated (Model) $PM_{2.5}$ concentrations Gangneung.

concentrations due to the approaching cold front.

3.4. Horizontal changes in $PM_{2.5}$ concentrations due to the cold front passage

Fig. 5 depicts the horizontal distribution of $PM_{2.5}$ concentrations over South Korea during and after the passage of the cold front for each stage, with the purpose of demonstrating the impact of the cold front on Gangneung's air quality. During both Stages 1 and 2, the $PM_{2.5}$ concentrations in Gangneung evidently increased after the passage of the cold front.

Prior to the passage of the cold front during Stage 1, high concentrations of $PM_{2.5}$ exceeding 75 $\mu g \cdot m^{-3}$ were observed along the western coast of the Korean Peninsula. $PM_{2.5}$ was transported by the southwestern winds, resulting in concentrations exceeding 60 $\mu g \cdot m^{-3}$ even in eastern areas after the cold front's passage.

Before the passage of the cold front during Stage 2, low concentrations below 30 $\mu g \cdot m^{-3}$ were observed in South Korea, excluding some regions (including Seoul). However, high concentrations exceeding 50 $\mu g \cdot m^{-3}$ were evident in the northwestern part of the Korean Peninsula. Nevertheless, after the passage of the cold front, strong southwestern winds transporting high-concentration $PM_{2.5}$ reached Gangneung, leading to concentrations exceeding 75 $\mu g \cdot m^{-3}$. Based on the horizontal distribution of $PM_{2.5}$ concentrations, an increase in concentration was confirmed in Gangneung after the passage of the cold front during Stages 1 and 2.

3.5. Vertical changes in $PM_{2.5}$ concentrations due to the cold front passage

To examine the vertical changes in $PM_{2.5}$ due to the passage of the cold front, vertical cross-sections of $PM_{2.5}$ and the equivalent potential temperature (EPT) along the A-B line in Fig. 1 are presented (Fig. 6).

Densely spaced EPT contour lines were present near the surface because of the cold air influx from the upper-layer associated with the passage of the cold front. Furthermore, during the passage of the cold front, Gangneung experienced low $PM_{2.5}$ concentrations below 30 $\mu g \cdot m^{-3}$, while high concentrations exceeding 70 $\mu g \cdot m^{-3}$ were observed near the 1 km altitude over the Yellow Sea (longitude 125.2°–125.7°) in both Stage 1 and Stage 2 over the f areas. After the cold front's passage, $PM_{2.5}$ concentrations in Gangneung increased to over 50 $\mu g \cdot m^{-3}$, surpassing the concentrations observed before the cold front's passage, and high concentrations were evident up to approximately 1500 m.

A previous study (Lee et al., 2019) suggested that when air pollutants are transported over a long range from upwind areas to the Korean Peninsula, they tend to be carried to the upper nocturnal boundary

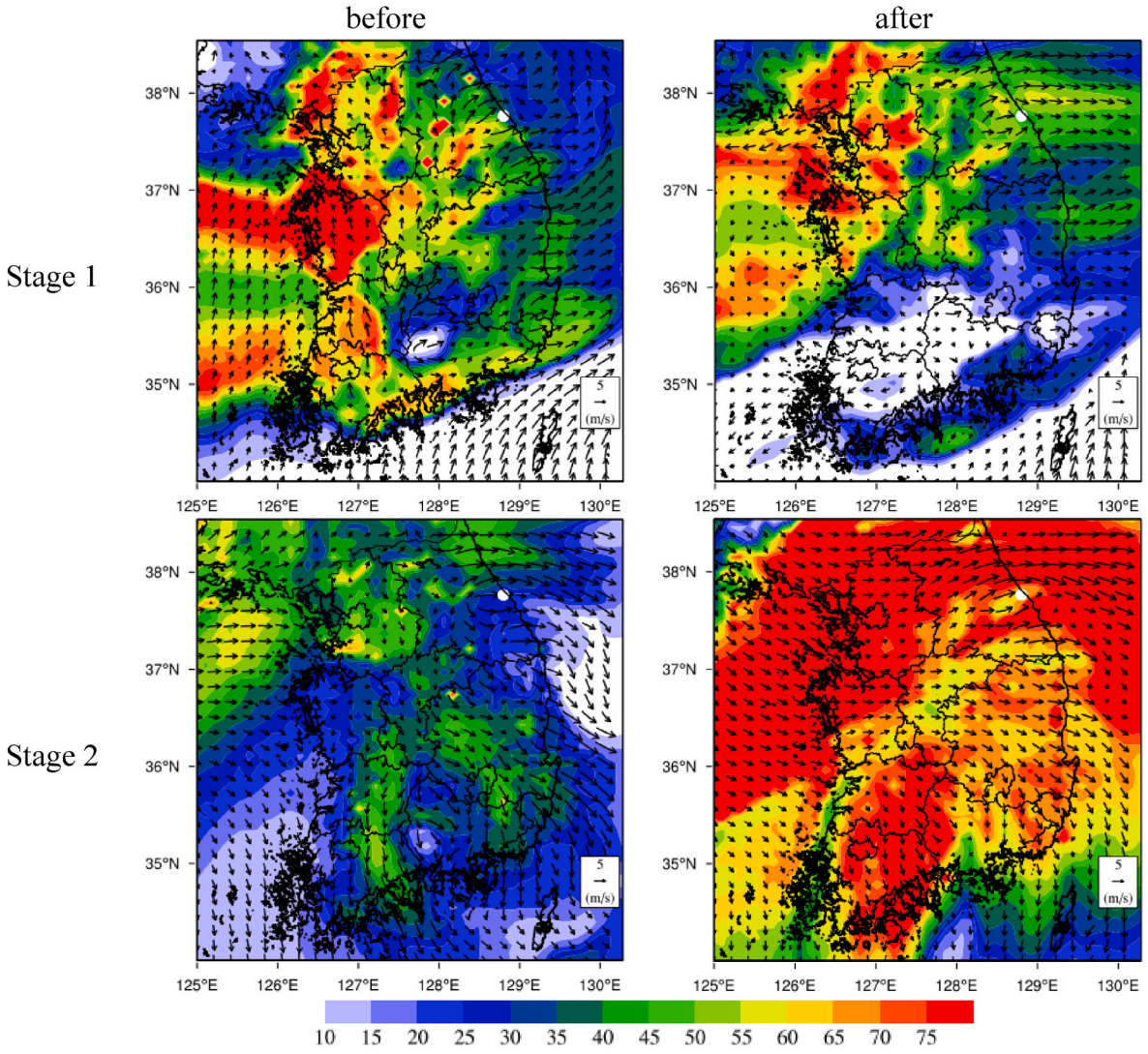


Fig. 5. Spatial distribution of $PM_{2.5}$ concentrations (unit: $\mu g \cdot m^{-3}$) before and after the passage of the cold front for (a) Stage 1 and (b) Stage 2. The white circle indicates the location of Gangneung.

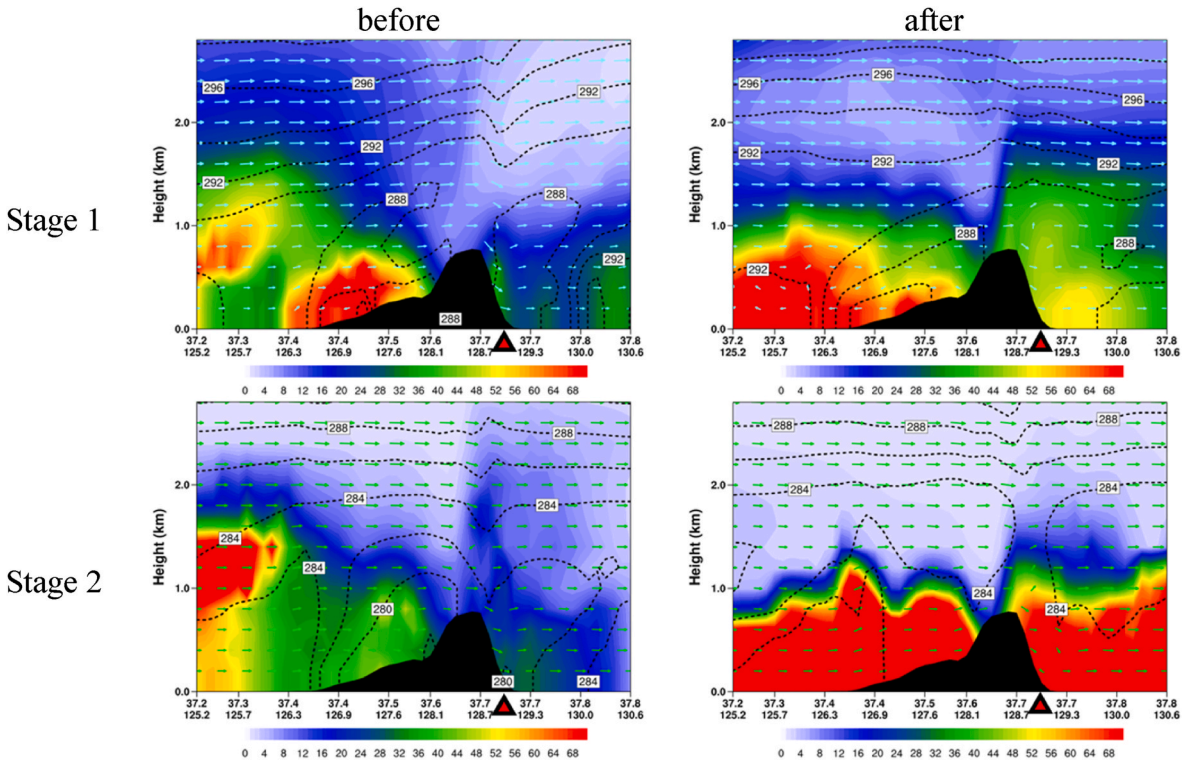


Fig. 6. Vertical cross-section (along the line A-B in Fig. 1) of the $PM_{2.5}$ concentrations (unit: $\mu g \cdot m^{-3}$) and equivalent potential temperature (black dash line, unit: K). Red triangle indicate Gangneung.

layer. During the episode period, daytime PBL heights were in the range of 800–1000 m (not shown). The high $PM_{2.5}$ concentrations observed at an altitude of 1.5 km appear to be influenced by long-range transport, considering the emission characteristics of Gangneung, which is located in a downwind area with limited local emissions, and the low daytime PBL heights.

Therefore, the high concentration of $PM_{2.5}$ observed near the 1 km altitude over the Yellow Sea appears to result from long-range transport from upwind regions.

Furthermore, the high $PM_{2.5}$ concentrations in the upper-layer of Gangneung are transported to the surface by downdrafts generated as air passes over elevated terrain, such as mountains or hills, contributing to an increase in surface concentrations.

3.6. Contributions of horizontal and vertical advection

A previous study (Zhang et al., 2022) suggested that air pollutants are transported downwind through advection during the passage of the cold front. Therefore, to analyze the horizontal and vertical advection processes that increase $PM_{2.5}$ concentrations in the Gangneung area during the passage of the cold front (Stage 1:06:00 to 09:00 LST on January 16, Stage 2:00:00 to 03:00 LST on January 20), an Integrated Process Rate (IPR) analysis was performed (Fig. 7). If the value of the advection process is positive, it indicates a contribution to the increase in $PM_{2.5}$ concentrations.

During Stages 1 and 2, the vertical advection (ZADV) process was positive up to an altitude of 200 m, whereas the horizontal advection (HADV) process displayed positive values above 200 m in altitude (Fig. 7). This result indicates that near the surface in Gangneung, $PM_{2.5}$ concentrations increased due to the ZADV process, while above 200 m altitude, concentrations increased due to the HADV process. During Stages 1 and 2, the patterns of the contributions from the HADV and ZADV processes were similar; however, the magnitude of $PM_{2.5}$ concentrations increases differed. The $PM_{2.5}$ concentrations increase due to the ZADV process near the surface was greater in Stage 2 (64 $\mu g \cdot m^{-3}$) than in Stage 1 (35 $\mu g \cdot m^{-3}$). The contribution difference of the ZADV

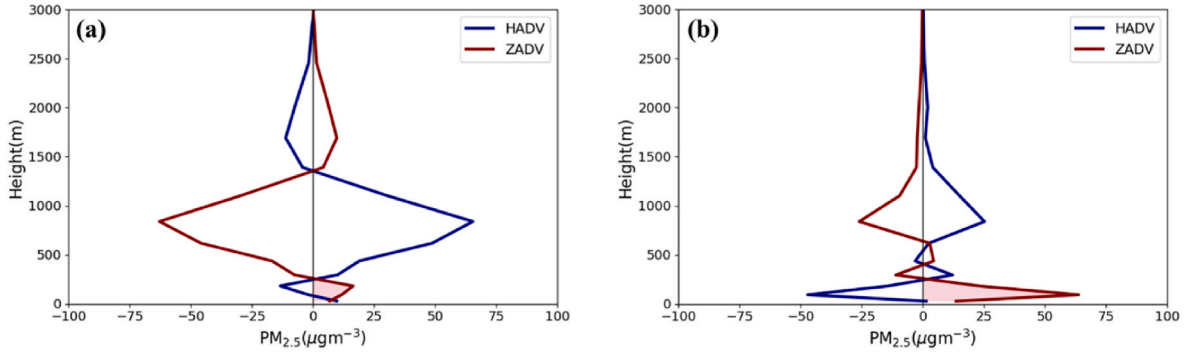


Fig. 7. Contribution of horizontal advection (HADV) and vertical advection (ZADV) processes to the $PM_{2.5}$ concentrations over Gangneung during the cold front passage for (a) Stage 1 and (b) Stage 2.

process may vary depending on the concentration of upper-layer air pollutants or the intensity of downdraft. As air moves over high-altitude areas, such as mountains or hills, it undergoes subsidence, resulting in the generation of downdraft air currents. These downdrafts can transport upper-layer pollutants to the surface, potentially affecting surface concentrations.

Fig. 8 displays the potential vertical temperature profiles for Stages 1 and 2 to examine the subsidence difference. During the passage of the cold front in the potential temperature vertical profiles, the atmosphere stabilized at night (indicated by an increase in the potential temperature at the same altitude), resulting in subsidence in the air. However, Stage 2 showed a greater amount of subsidence than Stage 1, and owing to this difference in subsidence, it appears that during Stage 2, more air pollutants were transported from the upper-layer to the surface via vertical advection.

3.7. Differences in synoptic patterns after the passage of the cold front

Subsidence airflows often occur under high-pressure systems with clear and stagnant meteorological conditions; hence, the amount of subsidence can vary depending on the synoptic meteorological conditions. Therefore, to examine the synoptic patterns over the Korean Peninsula following the passage of the cold front, we presented the horizontal distribution of the SLP (Fig. 9).

Stage 1 was dominated by a low-pressure system following the passage of the cold front, whereas Stage 2 was dominated by a high-pressure system. During Stage 1, the influence of a low-pressure system following the passage of the cold front resulted in precipitation primarily in the southern regions of the Korean Peninsula. The wet deposition effect of precipitation led to $PM_{2.5}$ concentrations below 20 $\mu g \cdot m^{-3}$ in the southern regions (Fig. 5 and Fig. S8). In contrast, during Stage 2, a high-pressure system developed behind the cold front, which accompanied the passage of the cold front.

Furthermore, during Stage 2, at 15:00 LST on the 20th day following the passage of the cold front, a temperature-inversion layer was observed below 300 m (Fig. S9). This, in combination with the influence of the high-pressure system and temperature inversion layer, may contribute to the accumulation of air pollutants near the surface. In contrast, during Stage 1, a mixed layer with minimal temperature variation up to 500 m altitude was observed following the passage of the cold front. These meteorological conditions are favorable for the daytime vertical dispersion of air pollutants.

In summary, the impact of air pollution resulting from the passage of a cold front varied according to the synoptic patterns developed after the passage of the cold front. Under the influence of high-pressure systems, stable atmospheric conditions combined with subsidence caused by high-altitude terrain features enhanced the vertical transport of air pollutants from the upper-layers to the surface. Additionally, the occurrence of temperature inversion near the surface can lead to the accumulation of air pollutants and the formation of high concentrations.

4. Summary and conclusion

This study analyzed the influence of winter cold front passages on $PM_{2.5}$ concentrations over the Korean Peninsula using WRF and CMAQ numerical models. This study investigated the synoptic patterns associated with high $PM_{2.5}$ concentration events (a total of 16 days) during the winter seasons from 2016 to 2022 in the Gangneung area. This region is characterized by limited local emissions and is located on the downwind side of high mountains.

Unlike the typical occurrence of air pollution under high-pressure systems, characterized by air stagnation and no precipitation, a synoptic pattern exists with a high-pressure system in the west and a low-pressure system in the east of the Korean Peninsula. Furthermore, the analysis revealed that on some high-concentration days (9 out of 16 days), the temperature was lower than that on the previous day, which was presumably influenced by the passage of the winter cold front.

The episode period was from January 14 to 23, 2018 and was characterized by severe air pollution associated with cold fronts and low-pressure systems. We classified this period into two stages: Stage 1, from January 16, 00:00 to 12:00 LST, and Stage 2, from January 19, 18:00 LST to January 20, 06:00 LST. Analysis of observational data for the episode period revealed meteorological changes, including 2-m temperature decreases and increases in 10-m wind speed and 2-m relative humidity, associated with the passage of the cold front. These changes were linked to the occurrence of peaks in $PM_{2.5}$ concentrations, suggesting the relevance of the cold front to the high $PM_{2.5}$ levels observed in Gangneung.

Meteorological changes and an increase in $PM_{2.5}$ concentrations resulting from the passage of the cold front were confirmed using the WRF and CMAQ models. The cold front led to a decrease in temperatures by 2–4 °C, primarily in the central regions of the Korean Peninsula. Furthermore, after the passage of the cold front, a high concentration of $PM_{2.5}$ in the nocturnal boundary layer above 1–1.5 km was transported, resulting in an increase in $PM_{2.5}$ concentrations exceeding 30 $\mu g \cdot m^{-3}$ in Gangneung. In the upper-layer, high-concentration $PM_{2.5}$ was transported from higher altitudes than the daytime PBL heights.

Considering the geographical characteristics of Gangneung, which has low local emissions and is situated downwind, it appears that high $PM_{2.5}$ concentrations in the upper-layer were transported from altitudes higher than the daytime PBL heights. Therefore, the influence appears to be due to long-range transport from upwind areas rather than vertical

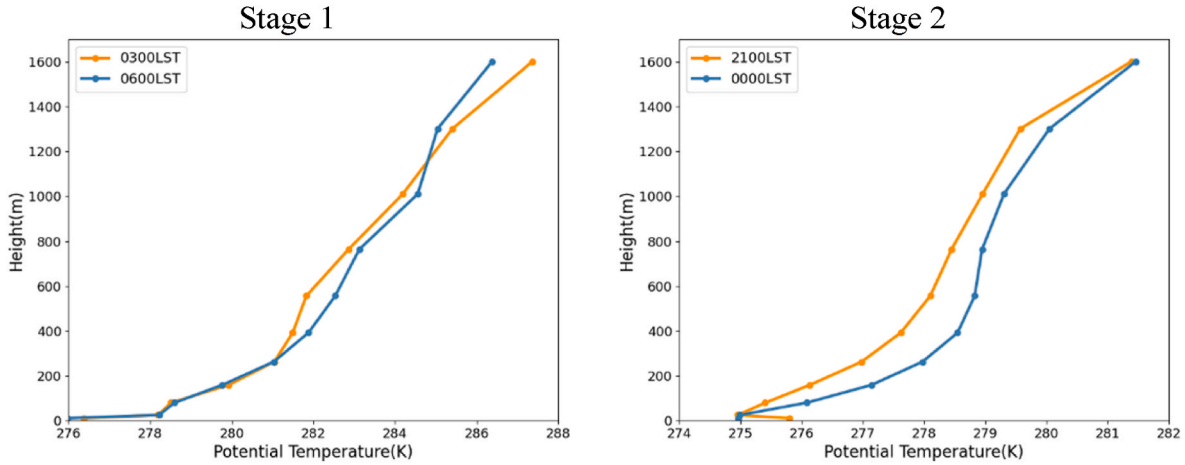


Fig. 8. Vertical profile of potential temperature at Gangneung.

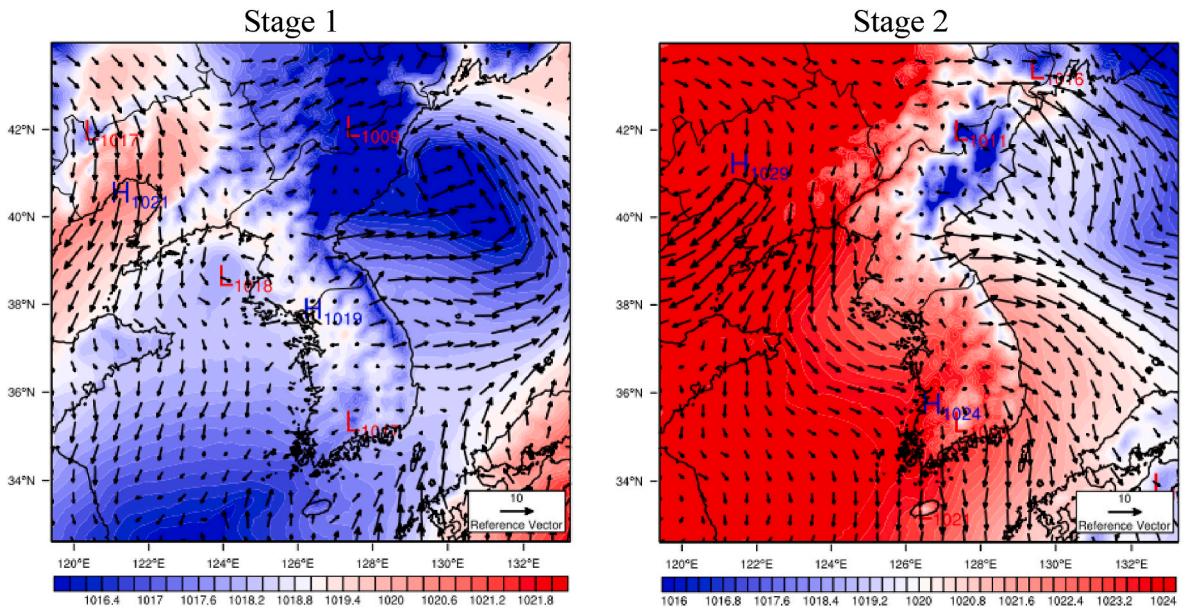


Fig. 9. Spatial distribution of sea level pressure (unit: hPa) after the cold front passage.

mixing. The contribution analysis using IPR revealed that $PM_{2.5}$ was transported to Gangneung by horizontal advection (HADV) in the upper-layer. Additionally, $PM_{2.5}$ was transported to the surface through a downdraft (vertical advection process, ZADV) due to air subsidence on the downwind side of high terrain. Particularly, the contribution of the ZADV process was significantly higher in Stage 2 (64 $\mu g \cdot m^{-3}$) compared to Stage 1 (35 $\mu g \cdot m^{-3}$). This can be attributed to the favorable meteorological conditions in Stage 2, influenced by the high-pressure system expanding behind the cold front, which facilitated air subsidence due to high-altitude areas and the accumulation of air pollutants due to temperature inversions, resulting in a greater increase in $PM_{2.5}$ concentrations.

This study contributes to a quantitative understanding of the advection processes of $PM_{2.5}$ before and after the passage of the cold front and sheds light on the mechanisms leading to high $PM_{2.5}$ concentrations in winter over the Korean Peninsula. Additionally, we investigated the potential for air pollution over the Korean Peninsula under non-stagnant meteorological conditions. Particularly, in Gangneung, located on the lee side with low local emissions, there was a significant increase in $PM_{2.5}$ transport from the surrounding areas before and after the passage of the cold front, resulting in severe air pollution. However, it is important to note that the relationship between synoptic patterns and air quality may vary depending on factors such as the spatiotemporal distribution of air pollutants, local emissions, and geographical characteristics. Hence, future studies should aim to enhance our understanding of the influence of synoptic patterns on regional meteorology and air quality under both stagnant and non-stagnant meteorological conditions on the Korean Peninsula. Furthermore, additional research is needed to understand the relationship between the decrease in anthropogenic emissions in upwind areas and the occurrence of severe air pollution due to the passage of cold fronts.

Funding

This research was supported by the Basic Science Research Program through the National Research Foundation of Korea (NRF), funded by the Ministry of Education (NRF-2020R1A6A1A03044834) and the Korean Government (MSIT) (No. 2022R1A2C1093229).

CRediT authorship contribution statement

Jung-Woo Yoo: Writing – original draft, Visualization, Validation, Methodology, Investigation, Data curation, Conceptualization. **Soon-Young Park:** Visualization, Validation, Investigation. **Hyun-Young Jo:** Software, Data curation. **Yeomin Jeong:** Software, Data curation. **Hyo-Jung Lee:** Resources, Data curation. **Cheol-Hee Kim:** Project administration, Conceptualization. **Soon-Hwan Lee:** Writing – review & editing, Supervision, Methodology, Investigation, Conceptualization.

Declaration of competing interest

The authors declare the following financial interests/personal relationships which may be considered as potential competing interests: Soon-Hwan Lee reports financial support was provided by South Korea Ministry of Science and ICT. Soon-Hwan Lee reports financial support was provided by South Korea Ministry of Education. If there are other authors, they declare that they have no known competing financial interests or personal relationships that could have appeared to influence the work reported in this paper.

Data availability

Data will be made available on request.

Appendix A. Supplementary data

Supplementary data to this article can be found online at https://doi.org/10.1016/j.envpol.2024.123803.

References

Agathokleous, E., Feng, Z., Oksanen, E., Sicard, P., Wang, Q., Saitanis, C.J., Araminiene, V., Blande, J.D., Hayes, F., Calatayud, V., Domingos, M., Veresoglou, S. D., Peñuelas, J., Wardle, D.A., de Marco, A., Li, Z., Harmens, H., Yuan, X., Vitale, M., Paoletti, E., 2020. Ozone affects plant, insect, and soil microbial communities: a threat to terrestrial ecosystems and biodiversity. Sci. Adv. 6, 1–18. https://doi.org/10.1126/sciadv.abc1176.

Apte, J.S., Brauer, M., Cohen, A.J., Ezzati, M., Pope, C.A., 2018. Ambient $PM_{2.5}$ reduces global and regional life expectancy. Environ. Sci. Technol. Lett. 5, 546–551. https://doi.org/10.1021/acs.estlett.8b00360.

Bae, M., Kim, B.U., Kim, H.C., Kim, J., Kim, S., 2021. Role of emissions and meteorology in the recent $PM_{2.5}$ changes in China and South Korea from 2015 to 2018. Environ. Pollut. 270 (2021), 116233 https://doi.org/10.1016/j.envpol.2020.116233.

Bei, N., Li, Xiaopei, Tie, X., Zhao, L., Wu, J., Li, Xia, Liu, L., Shen, Z., Li, G., 2020. Impact of synoptic patterns and meteorological elements on the wintertime haze in the Beijing-Tianjin-Hebei region, China from 2013 to 2017. Sci. Total Environ. 704, 135210 https://doi.org/10.1016/j.scitotenv.2019.135210.

Byun, D., Schere, K.L., 2006. Review of the governing equations, computational algorithms, and other components of the models-3 Community Multiscale Air Quality (CMAQ) modeling system. Appl. Mech. Rev. 59, 51–76. https://doi.org/10.1115/1.2128636.

Chen, Z., Xie, X., Cai, J., Chen, D., Gao, B., He, B., Cheng, N., Xu, B., 2018. Understanding meteorological influences on $PM_{2.5}$ concentrations across China: a temporal and spatial perspective. Atmos. Chem. Phys. 18, 5343–5358. https://doi.org/10.5194/acp-18-5343-2018.

Cohen, A.J., Brauer, M., Burnett, R., Anderson, H.R., Frostad, J., Estep, K., Balakrishnan, K., Brunekreef, B., Dandona, L., Dandona, R., Feigin, V., Freedman, G., Hubbell, B., Jobling, A., Kan, H., Knibbs, L., Liu, Y., Martin, R., Morawska, L., Pope, C.A., Shin, H., Straif, K., Shaddick, G., Thomas, M., van Dingenen, R., van Donkelaar, A., Vos, T., Murray, C.J.L., Forouzanfar, M.H., 2017. Estimates and 25-year trends of the global burden of disease attributable to ambient air pollution: an analysis of data from the Global Burden of Diseases Study 2015. Lancet 389, 1907–1918. https://doi.org/10.1016/S0140-6736(17)30505-6.

Ek, M.B., Mitchell, K.E., Lin, Y., Rogers, E., Grunmann, P., Koren, V., Gayno, G., Tarpley, J.D., 2003. Implementation of Noah land surface model advances in the National Centers for Environmental Prediction operational mesoscale Eta model. J. Geophys. Res. Atmos. 108, 1–16. https://doi.org/10.1029/2002jd003296.

Emery, C., Tai, E., Yarwood, G., 2001. Enhanced meteorological modeling and performance evaluation for two Texas ozone episodes. Env. Int. Corp. 235.

Gipson, G.L., Young, J., 1990. Science Algorithms of the EPA Models-3 Community Multiscale Air Quality (CMAQ) Modeling System. Process analysis, US EPA.

Hong, S.Y., Noh, Y., Dudhia, J., 2006. A new vertical diffusion package with an explicit treatment of entrainment processes. Mon. Weather Rev. 134, 2318–2341. https://doi.org/10.1175/MWR3199.1.

Hu, Y., Wang, S., Ning, G., Zhang, Y., Wang, J., Shang, Z., 2018. A quantitative assessment of the air pollution purification effect of a super strong cold-air outbreak in January 2016 in China. Air Qual. Atmos. Heal. 11, 907–923. https://doi.org/10.1007/s11869-018-0592-2.

Hu, X.M., Xue, M., Kong, F., Zhang, H., 2019. Meteorological conditions during an ozone episode in Dallas-Fort Worth, Texas, and impact of their modeling uncertainties on air quality prediction. J. Geophys. Res. Atmos. 124, 1941–1961. https://doi.org/10.1029/2018JD029791.

Hu, X.M., Hu, J., Gao, L., Cai, C., Jiang, Y., Xue, M., Zhao, T., Crowell, S.M.R., 2021. Multisensor and multimodel monitoring and investigation of a wintertime air pollution event ahead of a cold front over eastern China. J. Geophys. Res. Atmos. 126 https://doi.org/10.1029/2020JD033538.

Iacono, M.J., Delamere, J.S., Mlawer, E.J., Shephard, M.W., Clough, S.A., Collins, W.D., 2008. Radiative forcing by long-lived greenhouse gases: calculations with the AER radiative transfer models. J. Geophys. Res. Atmos. 113, 2–9. https://doi.org/10.1029/2008JD009944.

Itahashi, S., Uno, I., Osada, K., Kamiguchi, Y., Yamamoto, S., Tamura, K., Wang, Z., Kurosaki, Y., Kanaya, Y., 2017. Nitrate transboundary heavy pollution over East Asia in winter. Atmos. Chem. Phys. 17, 3823–3843. https://doi.org/10.5194/acp-17-3823-2017.

Jin, X., Cai, X., Huang, Q., Wang, X., Song, Y., Zhu, T., 2021. Atmospheric boundary layer-free troposphere air exchange in the North China Plain and its impact on $PM_{2.5}$ pollution. J. Geophys. Res. Atmos. 126, 1–18. https://doi.org/10.1029/2021JD034641.

Jun, M.J., Gu, Y., 2023. Effects of transboundary $PM_{2.5}$ transported from China on the regional $PM_{2.5}$ concentrations in South Korea: a spatial panel-data analysis. PLoS One 18, e0281988. https://doi.org/10.1371/journal.pone.0281988.

Kain, J.S., 2004. The Kain–Fritsch convective parameterization: an update. J. Appl. Meteorol. 43, 170–181.

Kang, H., Zhu, B., Liu, X., Shi, S., Hou, X., Lu, W., Yan, S., Pan, C., Chen, Y., 2021. Three-dimensional distribution of $PM_{2.5}$ over the Yangtze River Delta as cold fronts moving through. J. Geophys. Res. Atmos. 126, 1–11. https://doi.org/10.1029/2020JD034035.

Lee, H.J., Jo, H.Y., Kim, S.W., Park, M.S., Kim, C.H., 2019. Impacts of atmospheric vertical structures on transboundary aerosol transport from China to South Korea. Sci. Rep. 9, 1–9. https://doi.org/10.1038/s41598-019-49691-z.

Li, J., Chen, H., Li, Z., Wang, P., Cribb, M., Fan, X., 2015. Low-level temperature inversions and their effect on aerosol condensation nuclei concentrations under different large-scale synoptic circulations. Adv. Atmos. Sci. 32, 898–908. https://doi.org/10.1007/s00376-014-4150-z.

Liu, X.G., Li, J., Qu, Y., Han, T., Hou, L., Gu, J., Chen, C., Yang, Y., Liu, X., Yang, T., Zhang, Y., Tian, H., Hu, M., 2013. Formation and evolution mechanism of regional haze: a case study in the megacity Beijing, China. Atmos. Chem. Phys. 13, 4501–4514. https://doi.org/10.5194/acp-13-4501-2013.

Liu, Y., Wang, B., Zhu, Q., Luo, R., Wu, C., Jia, R., 2019. Dominant synoptic patterns and their relationships with $PM_{2.5}$ pollution in winter over the beijing-tianjin-hebei and yangtze river delta regions in China. J. Meteorol. Res. 33, 765–776. https://doi.org/10.1007/s13351-019-9007-z.

Liu, X., Zhu, B., Kang, H., Hou, X., Gao, J., Kuang, X., Yan, S., Shi, S., Fang, C., Pan, C., Meng, K., 2021. Stable and transport indices applied to winter air pollution over the Yangtze River Delta, China. Environ. Pollut. 272, 115954 https://doi.org/10.1016/j.envpol.2020.115954.

Lu, M., Tang, X., Wang, Z., Wu, L., Chen, X., Liang, S., Zhou, H., Wu, H., Hu, K., Shen, L., Yu, J., Zhu, J., 2019. Investigating the transport mechanism of $PM_{2.5}$ pollution during january 2014 in wuhan, Central China. Adv. Atmos. Sci. 36, 1217–1234. https://doi.org/10.1007/s00376-019-8260-5.

Ma, S., Xiao, Z., Zhang, Y., Wang, L., Shao, M., 2020. Assessment of meteorological impact and emergency plan for a heavy haze pollution episode in a core city of the north China plain. Aerosol Air Qual. Res. 20, 26–42. https://doi.org/10.4209/aaqr.2019.08.0392.

Miao, Y., Guo, J., Liu, S., Liu, H., Li, Z., Zhang, W., Zhai, P., 2017. Classification of summertime synoptic patterns in Beijing and their associations with boundary layer structure affecting aerosol pollution. Atmos. Chem. Phys. 17, 3097–3110. https://doi.org/10.5194/acp-17-3097-2017.

Mo, J., Gong, S., Zhang, L., He, J., Lu, S., Zhou, Y., Ke, H., Zhang, H., 2021. Impacts of long-range transports from Central and South Asia on winter surface $PM_{2.5}$ concentrations in China. Sci. Total Environ. 777, 146243 https://doi.org/10.1016/j.scitotenv.2021.146243.

Morrison, H., Thompson, G., Tatarskii, V., 2009. Impact of cloud microphysics on the development of trailing stratiform precipitation in a simulated squall line: comparison of one- and two-moment schemes. Mon. Weather Rev. 137, 991–1007. https://doi.org/10.1175/2008MWR2556.1.

Pateraki, S., Asimakopoulos, D.N., Flocas, H.A., Maggos, T., Vasilakos, C., 2012. The role of meteorology on different sized aerosol fractions (PM_{10}, $PM_{2.5}$, $PM_{2.5\text{-}10}$). Sci. Total Environ. 419, 124–135. https://doi.org/10.1016/j.scitotenv.2011.12.064.

Skamarock, W.C., Klemp, J.B., Dudhia, J., Gill, D.O., Barker, D.M., Duda, M.G., Huang, X.-Y., Wang, W., Powers, J.G., 2008. A Description of the Advanced Research WRF Version3. National Center for Atmospheric Research Technical Note. NCAR, Boulder. http://www.mmm.ucar.edu/wrf/users/docs/arw_v3.pdf.

Tai, A.P.K., Mickley, L.J., Jacob, D.J., 2010. Correlations between fine particulate matter ($PM_{2.5}$) and meteorological variables in the United States: implications for the sensitivity of $PM_{2.5}$ to climate change. Atmos. Environ. 44, 3976–3984. https://doi.org/10.1016/j.atmosenv.2010.06.060.

Yoo, J.W., Park, S.Y., Lee, K., Lee, D., Lee, Y., Lee, S.H., 2022. Impacts of plateau-induced lee troughs on regional $PM_{2.5}$ over the Korean Peninsula. Atmos. Pollut. Res. 13, 101459 https://doi.org/10.1016/j.apr.2022.101459.

Yu, C., Zhao, T.L., Bai, Y.Q., Zhang, L., Kong, S.F., Yu, X.N., He, J.H., Cui, C.G., Yang, J., You, Y.C., Ma, G.X., Wu, M., Chang, J.C., 2020. Heavy air pollution with a unique "non-stagnant" atmospheric boundary layer in the Yangtze River middle basin aggravated by regional transport of $PM_{2.5}$ over China. Atmos. Chem. Phys. 20, 7217–7230. https://doi.org/10.5194/acp-20-7217-2020.

Zeng, Q., Cheng, X., Hu, F., Peng, Z., 2010. Gustiness and coherent structure of strong winds and their role in dust emission and entrainment. Adv. Atmos. Sci. 27, 1–13. https://doi.org/10.1007/s00376-009-8207-3.

Zhang, H., Yuan, H., Liu, X., Yu, J., Jiao, Y., 2018. Impact of synoptic weather patterns on 24 h-average $PM_{2.5}$ concentrations in the North China Plain during 2013–2017. Sci. Total Environ. 627, 200–210. https://doi.org/10.1016/j.scitotenv.2018.01.248.

Zhang, Q., Zheng, Y., Tong, D., Shao, M., Wang, S., Zhang, Y., Xu, X., Wang, J., He, H., Liu, W., Ding, Y., Lei, Y., Li, J., Wang, Z., Zhang, X., Wang, Y., Cheng, J., Liu, Y., Shi, Q., Yan, L., Geng, G., Hong, C., Li, M., Liu, F., Zheng, B., Cao, J., Ding, A., Gao, J., Fu, Q., Huo, J., Liu, B., Liu, Z., Yang, F., He, K., Hao, J., 2019. Drivers of improved $PM_{2.5}$ air quality in China from 2013 to 2017. Proc. Natl. Acad. Sci. USA 116 (49), 24463–24469. https://doi.org/10.1073/pnas.1907956116.

Zhang, W., Li, W., An, X., Zhao, Y., Sheng, L., Hai, S., Li, X., Wang, F., Zi, Z., Chu, M., 2022. Numerical study of the amplification effects of cold-front passage on air pollution over the North China Plain. Sci. Total Environ. 833, 155231 https://doi.org/10.1016/j.scitotenv.2022.155231.

Zheng, B., Tong, D., Li, M., Liu, F., Hong, C., Geng, G., Li, H., Li, X., Peng, L., Qi, J., Yan, L., Zhang, Y., Zhao, H., Zheng, Y., He, K., Zhang, Q., 2018. Trends in China's anthropogenic emissions since 2010 as the consequence of clean air actions. Atmos. Chem. Phys. 18 (19), 14095–14111. https://doi.org/10.5194/acp-18-14095-2018.